Ultra-fast, Energy-efficient synthesis of Intermetallics; Microwave-Induced Metal Plasma (*MIMP*) Synthesis of Mg_2Sn

Zhen Fan[1], Mauro Davide Cappelluti[1,2], Duncan H. Gregory[1]*

1. WestCHEM, School of Chemistry, Joseph Black Building, University of Glasgow, Glasgow, G12 8QQ, United Kingdom

2. School of Engineering, Rankine Building, University of Glasgow, Glasgow, G12 8QQ, United Kingdom

** Correspondence: Duncan.Gregory@glasgow.ac.uk; Tel.: +44-141-330-8128*

Abstract

Magnesium stannide, Mg_2Sn, can be synthesised from the elements using microwaves over minute timescales in the solid state. The effects of Mg content, pressure and microwave irradiation time have been investigated and single phase Mg_2Sn is produced in 1 min under only 200 W of incident irradiation *in vacuuo* ($P < 10^{-6}$ mbar). The fine Mg and Sn metal powders both couple efficiently with the microwave field under vacuum, heating rapidly and generating plasma. The metal plasma formation is shown to be essential for reaction completion and promotes the enhanced kinetics of the reaction *via* one or more possible reaction pathways to sintered Mg_2Sn. This approach provides a simple, ultra-fast, sustainable and energy-efficient route to phase-pure Mg_2Sn, a material that is extremely challenging to make at high purity by conventional methods. The *MIMP* formalism should be applicable to many other metalloid materials of this and other types.

Keywords: magnesium stannide, microwaves, plasma, ultra-fast synthesis, energy-efficient

Introduction

The demands for low-carbon (or even carbon-free) and ecologically clean power generation from renewable sources and for maximising the energy efficiency of industrial processes are ever-increasing. These demands provide the impetus for sustainable synthesis and manufacturing technologies of energy-conversion/storage materials, which themselves are low-cost and Earth-abundant [1-5]. Magnesium stannide (Mg_2Sn) is an intermetallic semiconductor belonging to the family of compounds Mg_2X (X= Si, Ge, Sn and Pb) [6]. Mg_2Sn together with Mg_2Si, Mg_2Ge and their solid solutions derived from various combinations of p-block elements (*e.g.* $Mg_2Si_xSn_{1-x}$, $Mg_2Sn_xGe_{1-x}$, and $Mg_2Si_xSn_{1-x-y}Ge_y$), have emerged as a promising class of thermoelectric materials for waste heat recovery at a mid-temperature range with light-weight, abundant and non-toxic constituent elements [7-13]. These materials show large Seebeck coefficients, high electrical conductivities, low thermal conductivities and ZT values exceeding unity [7-13]. A theoretical study has claimed Mg_2Sn exhibits the highest ZT value at 800 K among Mg_2X compounds (X = Si, Ge and Sn) and that this value of 1.1 arises from a minimisation of the lattice thermal conductivity [14]. Due to the prevalence of narrow band gaps in Mg_2X semiconductors, Mg_2Sn and Mg_2Si have also been considered as good candidates for infrared optoelectronic devices [15]. Additionally, magnesium ion batteries (MIBs), with the benefit of an Earth-abundant working cation (Mg^{2+}), have received considerable attention as potential long term replacements for Li-ion technologies. In this context, Mg_2Sn has attracted interest over the last 2 years as an emerging magnesiated-state anode material for the reversible storage of Mg^{2+} ions because of its high theoretical capacity, the relatively low potential for Mg^{2+}-insertion into Sn and its compatibility with a wider selection of electrolytes than Mg metal anodes themselves [16-20].

One of the chief reasons that the development of Mg_2Sn (or other Mg_2X compounds) is hindered as a sustainable energy material of choice, is its difficult and time-consuming synthesis. Large energy barriers need to be overcome for the diffusion of the metallic reactants in the solid state. Mg_2Sn is normally synthesised by conventional high temperature solid-state methods[7, 20], but can also be prepared *via* spark plasma sintering (SPS), or mechanical alloying methods[21-27]. Thermal reactions are complicated by the easy volatilization and oxidation of Mg and the aggregation of Sn during the long-duration, high-temperature synthesis process, thus annealing or multi-step treatments may be necessary [7, 20, 21, 22]. By contrast, room temperature synthesis by mechanical alloying offers a less energy-intensive alternative but still requires a long processing time with the possibility of

introducing contaminants and forming multi-phase products (and even metastable Mg_2Sn phases, which while fundamentally of significant interest can make selectivity and reproducibility difficult) [16, 23-27]. In fact, the mechanical alloying of the ductile-ductile Mg-Sn binary system often requires the addition of process control agents (PCAs), usually organic additives like octane and stearic acid, to prevent "sticking" and "caking" [16, 28]. In these circumstances, self-ignition induced by the PCA is possible. Moreover, the presence of a PCA can be detrimental to the properties of Mg_2X materials, necessitating the removal of the agent from the final products [16, 28]. Conversely, SPS is a very promising processing route that can eliminate sources of impurity such as PCAs without requiring the long heating times of conventional high-temperature methods [29]. Unfortunately, high-cost specialist equipment is essential and energy-expenditure is still relatively high since thermal treatments involving melting and/or annealing of the starting materials prior to the SPS process are often needed [29]. In fact, it is critical to maintain short SPS processing times to avoid the possible oxidation of the synthesised products. To varying extents, although mechanochemical and SPS methods offer distinct advantages, all the above-mentioned methods are either time consuming, energy consuming and/or lead to products often containing elemental *X* impurities (such as Sn in Mg_2Sn synthesis) or oxidised magnesium (MgO) [7, 16, 20, 21-29].

With an appropriate choice of conditions, application of microwave (MW) methods to materials synthesis can yield high-purity products sustainably and economically, offering rapid processing, increased energy efficiency and reduced equipment cost as compared to conventional high temperature methods [2-5]. The fast conversion of the absorbed MW energy into heat allows an instantaneous volumetric heating in the irradiated material [2-5, 30, 31]. Bulk metals generally reflect MWs due to their small skin depth. MWs cannot penetrate deep into the metal bulk and only the surface undergoes heating with a typical penetration depth of several microns [30, 31]. Reducing metal powders to particle sizes commensurate with the skin depth dramatically improves the absorption of MWs and can induce very high heating rates [32, 33]. Although the electrical interactions of microwaves with matter are usually defining, it has been suggested that the effect of *magnetic* loss in such fine metal powders can also contribute to efficient MW heating [31]. Although no single theory can precisely explain all the different possible interactions between MWs and materials [30, 31], the rapid MW heating of powders can be utilised reproducibly in solid-state MW syntheses, either by direct microwave heating or by "hybrid" microwave heating ("microwave-assisted heating") with the introduction of susceptors; a host of inorganic materials such as carbides, borides, halides,

nitrides, chalcogenides, metal clusters and intermetallic compounds can be prepared in this way[2-5, 34-36]. Equally, the method can be used purely for processing, such as in the sintering of metals or ceramics [37, 38]. MW-treated materials can exhibit a variety of morphologies from nanostructured particles through powders to solid ingots depending on the materials systems investigated and the experimental/instrumental design.

The very limited examples of solid-state MW reactions involving Sn were usually performed under vacuum in sealed ampoules (*e.g.* synthesis of Sn-Se Zintl phases, $Li_{17}Sn_4$ alloy and doped stannides, TiNiSn) [39-43]. Mg-containing main group alloys and compounds can also be synthesised in the solid state using MWs. These include the diboride superconductor MgB_2 and Mg_2Si-based thermoelectric materials [44-46]. Typically, high incident power MWs are required for tens of minutes under an inert gas atmosphere. The successful production of nano-powders of Mg_2Si sets an encouraging precedent for the MW synthesis of Mg_2X phases and in this case, pucks of Mg and Si powders that had been ball milled for two hours were heated using an incident microwave power of only 175 W for two minutes under nitrogen [47]. Interestingly, it was proposed that Mg does not significantly absorb microwaves during the Mg_2Si synthesis whereas silicon acts as a microwave susceptor during the reaction [47].

To date, no solid-state MW synthesis of any other Mg_2X phase has been reported. Herein, we report the first ultra-fast and energy-efficient solid-state MW synthesis of phase-pure Mg_2Sn. Whereas plasma formation has been reported in the MW synthesis of some metal chalcogenides and intermetallic compounds under vacuum, no equivalent reactions of this type have been reported for silicides or stannides and the influence of plasma formation in the synthesis of solid state materials remains largely unexplored [34-36]. We demonstrate that the contribution of plasma generation is likely to be profound in enabling the ultra-fast MW reaction of Mg_2Sn to proceed. In an effort both to optimise the MW reaction process and to appreciate the role of plasma in Mg_2Sn formation, we have studied the effects of varying experimental parameters on the progress of the stannide synthesis. The resulting observations have allowed us to propose potential MW interaction and reaction mechanisms towards magnesium intermetallics.

Experimental

Materials synthesis

Sample preparation was entirely performed inside an Ar-fed LABstar glovebox (mBRAUN) with an operating pressure of 2.3 mbar and H_2O and O_2 concentrations typically below 0.5 ppm. Mg (99.8%, 325 mesh, Alfa-Aesar) and Sn (99.5%, 10μm, Sigma-Aldrich) powders were weighed and mixed thoroughly in the ratios indicated in Table **1** and transferred into an alumina crucible (which can be considered MW-transparent). The crucible was placed at the bottom of a quartz tube with adjustable Swagelok sealing accessories and a quick-fit tap. The quartz tube was closed in the glovebox and then connected to a vacuum line, with pressure measured by a Pirani Gauge. This reaction setup is shown in Figure **1** and was designed to allow implementation of four very different gas pressure regimes. At one extreme, a closed quartz tube transferred directly from the recirculating glovebox provided an Ar atmosphere at *ca.* 1 bar. A pressure of 1.2×10^{-1} mbar was generated by opening the tap to the vacuum line and using the rotary pump only. A reduced pressure of $P \leq 10^{-6}$ mbar was generated in the reaction tube by utilising a vacuum line configuration connecting a turbomolecular pump in series with the rotary pump. Alternatively, a static vacuum was achieved by closing the quick-fit tap once the desired vacuum conditions were achieved prior to the start of the experiment.

A modified single-mode cavity MW reactor (CEM Discovery, 2.45 GHz) with an adjustable input power from 0 - 300 W was used for solid-state synthesis. The reaction tube was inserted inside the reactor such that the alumina crucible is located at the centre of the cavity. MW irradiation of 200 W was applied for different reaction times, spanning from 5-80 s under different vacuum conditions (Table **1**). Following irradiation, the quartz tube was naturally cooled to room temperature. Mg_2Sn is reported to be air-stable, even after months of exposure to atmospheric conditions [48]. Our observations and characterisation results suggested the same, but due to the unknown air-sensitivity of other potential products and the likelihood of the aerial oxidation/hydration of any unreacted Mg, the closed quartz reaction tube was transferred directly to the glovebox after cooling in each case. All the ground samples were then stored in the Ar-filled glovebox for further characterisation.

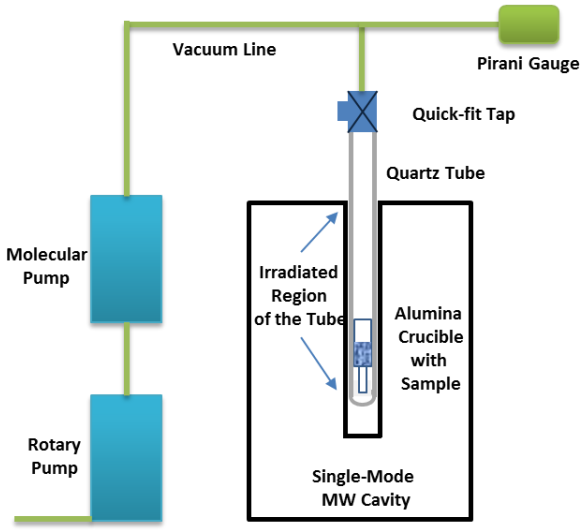

Figure 1. Experimental setup for the solid-state MW synthesis of Mg_2Sn.

Materials characterisation

Powder X-ray Diffraction (PXD) was performed using a PANalytical X'pert Pro MPD diffractometer in Bragg-Brentano geometry with Cu-$K_{\alpha 1}$ radiation (λ = 1.5406 Å), operating at an accelerating voltage and an emission current of 40 kV and 40 mA, respectively. PXD patterns were collected at room temperature over a 2θ range of 15-85 ° with a step size of either 0.0167 ° or 0.0334 ° and 55 s per step. The potentially air sensitive samples were loaded in the glove box into a bespoke aluminium sample holder consisting of a sealed chamber equipped with a Mylar window [49]. Previously published Mg_2Sn, Sn and Mg structures were used as initial model structures for Rietveld refinements [50, 51], which were performed by using GSAS through the EXPGUI interface [52]. However, for the phase-pure sample (Experiment **8**), a PXD pattern was also collected at a 0.0167 ° step size over 15-120 ° (2θ) range for a longer time (150 s per step) with the related Rietveld refinement performed by using JANA 2006 [53] (Figure **2a**).

Scanning Electron Microscopy (SEM) and Energy Dispersive X-ray Spectroscopy (EDX) were performed with a Philips/FEI XL30 ESEM (beam voltage 20 kV, maximum magnification 20 k) equipped with an INCA X-Act detector (Oxford Instruments Analytical, UK). Raman spectroscopy was performed over an effective Raman shift range of 50 - 500 cm^{-1} by using a LabRAM HR confocal microscope (Horiba Ltd., Kyoto, Japan) system with a variable optical hole aperture (100 - 300 μm), 600 mm^{-1} grating and a Synapse CCD detector. The excitation source was a Nd:YAG second harmonic laser (Ventus532, Laser Quantum, λ emission = 532 nm, output power 50 mW-1.5W). Thermogravimetric-differential thermal

analyses (TG-DTA) were performed using a Netzsch STA 409 PC instrument located in an Ar-fed MBraun glovebox (<0.1 ppm H_2O, <0.1 ppm O_2). Approximately 15 mg of Mg_2Sn sample from Experiment **8** was heated to 700 ^oC at a heating rate of 5 ^oC/min in an alumina pan under flowing Ar (60 mL/min).

Results

In a typical synthesis reaction, a mixture of Mg and Sn (in most cases in a 2.3:1 molar ratio) was contained in a quartz tube which was closed under vacuum ($P < 10^{-6}$ mbar). The reaction vessel was irradiated by MWs for varying durations, typically of 60 s or less (Table **1**). Plasma formed within a few seconds of applying MW radiation (Supporting Information Video **1**), which was an indication of the immediate interaction between the metal powders and the MWs as soon as incident power was supplied. The colour of the plasma turned from an initial pale-bright purple to brilliant green as the reaction proceeded. Under these conditions (Experiment **8**, Table **1**), the MW reaction generates crystalline, phase-pure cubic Mg_2Sn as observed by powder X-ray diffraction (PXD) (PDF # 01-071-9596, Figure 2a) [50]. PXD patterns presented no evidence of any oxidation of the synthesised product. Repeatable preparation of high-purity Mg_2Sn is dependent on certain, well-defined parameters, as indicated by the different conditions and resulting products in Table **1**, respectively. Higher purity materials tend to be formed at higher vacuum (lower pressures).

Rietveld refinement against PXD data (Figure **2a**, Tables **2**, **3**) confirmed the cubic fluorite structure (space group $Fm\bar{3}m$), where Mg is at the 8*c* (1/4, 1/4, 1/4) site and Sn is at the 4*a* (0, 0, 0) site (a = 6.7653(1) Å, Figure **2b**).The synthesised Mg_2Sn appears as an inhomogeneous mixture of larger pieces (with a metallic appearance, which is possibly caused by the melting of the product) and fine powders of a blueish colour [48]. The condensed pieces (Figures **2c** and **S11**) were brittle and could be easily ground into micron-size particles. The SEM images of the ground sample (Figure **2d**) shows clearly faceted fragments, indicating that the MW-synthesised product is highly crystalline. Finer particles of spheres and sub-micrometric fragments could also be observed in some SEM images, which were probably formed under the effect of the observed plasma [35]. EDX spectra taken across both the larger chunks and the ground sample (Figures **2e** and **S11**) consistently confirmed Mg/Sn atomic ratios of 2.0 ± 0.1 in excellent agreement with the theoretical composition of Mg_2Sn. Only one major peak, at 214.5 cm^{-1}, was observed in the Raman spectrum (Figure **S1**), which corresponds to the reported longitudinal optical mode band in bulk Mg_2Sn at 222 cm^{-1} [54]. An almost negligible

weight change (< 0.1-0.4 wt % across samples) occurred over the experimental temperature range according to the TG-DTA results (Figure S**2a**). No endothermic peaks relating to the melting of Sn or Mg could be detected [21]. The data support the thermal stability of the synthesised product, although coupled with the suggestion of Mg-deficiency from the Rietveld refinement of **8**, it is possible that small amounts of Mg are lost from Mg_2Sn at high temperature.

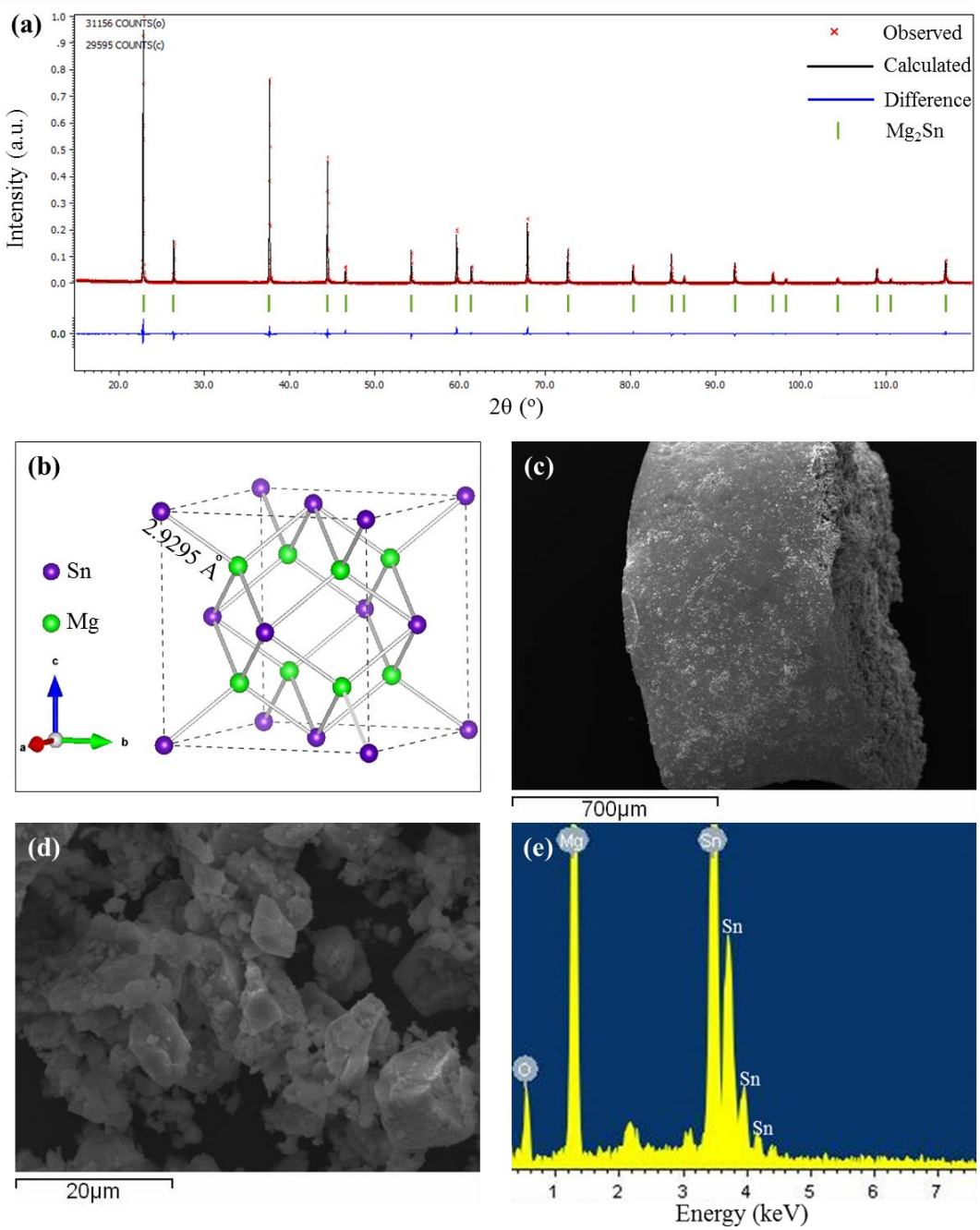

Figure 2. Characterisation of a typical Mg_2Sn sample synthesised at 200 W for 60 s in which the quartz reaction tube is initially closed under a static vacuum P < 10^{-6} mbar (Experiment **8**, Table **1**): (a) profile plot from Rietveld refinement; (b)

refined crystal structure; (c) SEM image of one condensed metallic piece; (d) SEM image of the ground powders; and (e) A representative EDX spectrum taken from the surface of the particles shown in (d).

Effect of Mg Content

MW irradiation of Mg and Sn powders individually under vacuum leads in the former case to the expected sublimation of Mg, in the latter case to sublimation of tiny amounts of Sn and in both cases to re-deposition of the elements on the walls of the quartz tubes on cooling (Figure **S4**, Figure **S5**, Supporting Information Video **3**, Supporting Information Video **4**). In light of these observations, an excess Mg content in the starting material is needed to account for Mg loss as has been reported in previous conventional syntheses of Mg_2Sn under inert gas atmospheres [7, 20, 21, 22, 29]. Using excess Mg representing 105 – 120 % of the stoichiometric molar amount (Experiments **1-4**, Table **1**) was investigated in various dynamic vacuum ($P< 10^{-6}$ mbar) syntheses in order to assess how much would be required to counteract the loss of reactant and to optimise the reaction towards single-phase product.

Unlike the "optimum" synthesis described above (Experiment **8)**, the products from experiments **1 - 4** were composed only of fine powders when using a dynamic vacuum ($P < 10^{-6}$ mbar). The observation of plasmas was noted in each case. The PXD patterns and the Rietveld refinements results (Table **1**, Figures **3**, **S12e & f**) indicate that a 2.3:1 Mg:Sn molar ratio provides a product purity of 98.4(1) wt%, compensating for much of the volatilisation of Mg. A further excess of Mg content to 2.4 molar equivalents did not increase the purity of the product any further, however (and a 2.3:1 Mg:Sn ratio was maintained in all subsequent experiments, Figure **S17**). The deviation of Mg_2Sn phase purity from 100% in the products might be attributed to the higher rates of sublimation of Mg over Sn. As Mg interacts with the electromagnetic field it transforms into plasma. The ionised Mg could then react with the quartz tube in the hotter irradiated region or re-condense/redeposit on the quartz tube walls towards the top of the reaction vessel, where the temperature begins to fall below the melting point of Mg (650 °C [21]).

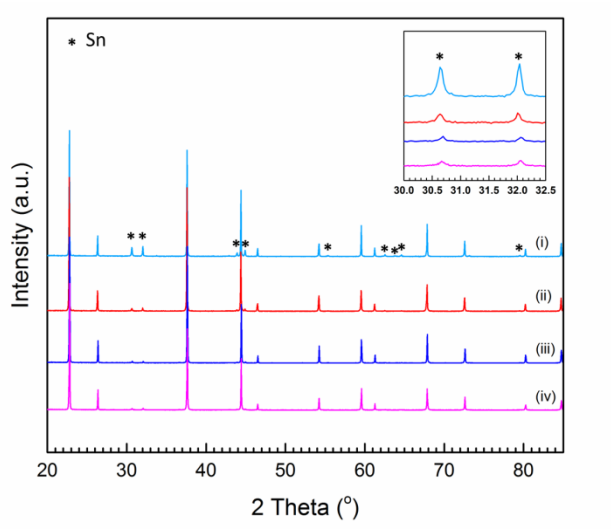

Figure 3. PXD patterns showing all products obtained with (i) 105 mol%, (ii) 110 mol%, (iii) 115 mol% and (iv) 120 mol% Mg under a dynamic vacuum ($P < 10^{-6}$ mbar) (Inset: PXD patterns from 30 – 32.5° (2θ) highlighting the intensity changes of the principal Sn (black marker) impurity peaks).

Effect of Pressure Conditions

Pressure has emerged as an essential parameter in the MW reaction in this work, affecting the stability of the plasma and the change in the physical states of the metallic species. During the reaction performed under Ar atmosphere at approximately 1.002 bar (Experiment **7**, Table **1**), no plasma was observed for the entire irradiation period (60 s). The reaction led to synthesis of minimal Mg_2Sn (12(1) wt% by Rietveld refinement) with most of the initial metal powders remaining unreacted as can be seen from the PXD results (Table **1,** Figures **4** and **S6a**). The analysis of the final product revealed no sign of melting or of the formation of agglomerates of metals. It is reasonable to assume that at atmospheric pressure under an inert atmosphere, there is no substantial MW heating of the metal powders; the reaction temperature is unlikely to reach the melting point of Sn (232 °C [21]). In a further experiment conducted under Ar (1.002 bar) in which the starting materials were irradiated at the same incident power for half the duration (30 s; experiment **19**), no formation of Mg_2Sn was observed and only the starting materials were detected by PXD (Table **1,** Figure **S6b**).

Experiments conducted under reduced pressure (with all other parameters unchanged; Experiments **3**, **5**, **6** and **8**, Table **1**) all led to the formation of plasma. These reactions present much higher yields of Mg_2Sn than those performed under an Ar (Experiments **7** and **19**; Figure **4**, Table **1**). It is probable that the initiation of the plasma indicates the requisite reaction conditions with a possible interaction mechanism involving the MW field-induced plasma and solid reactants. This promoted further experiments to investigate the influence of

the plasma and the behaviour of the individual Mg and Sn powders by MW irradiation under vacuum (Figure **S4**, Figure **S5**, Supporting Information Videos **3** and **4**). Both Mg and Sn individually couple efficiently with the electromagnetic field. The interaction of each metal independently with the field creates a plasma and deposited/condensed metal was observed on the walls of the quartz tube in each case. These observations indicate fast heating, vaporization and potentially ionisation of the metal vapours, leading to plasma initiation. Since plasmas are hot ionised media of fast-moving positively charged ions and faster-moving negatively charged electrons, they will be strongly influenced by both the high-frequency electrical and magnetic components of the MW field, promoting fast mass transfer and high heating rates [55, 56]. The formation of plasma during these MW reactions inevitably introduces alternative reaction mechanisms to those which occur solely in the solid state and provide routes to increase the rate at which Mg_2Sn is formed.

The variations in pressure and the type of the vacuum applied (*i.e.* dynamic *vs* static) affect the purity and form of the final products (Figure **4**, Table **1**). According to Rietveld refinement results, higher vacuum levels ($P < 10^{-6}$ mbar) lead to higher phase fractions of Mg_2Sn (Table **1**). Phase-pure Mg_2Sn could be obtained when the synthesis was conducted under a static vacuum ($P < 10^{-6}$ mbar, experiment **8**) and a dynamic vacuum condition of $P < 10^{-6}$ mbar (Experiment **3**) can also lead to high Mg_2Sn purity (phase fraction of 98.4(1) wt%). The morphology of the product also appears to exhibit a pressure-dependence. Metallic pieces (possibly caused by melting of the products) mixed with fine powders were observed for the reactions under a static vacuum of $P < 10^{-6}$ mbar (Experiment **8**), a static vacuum of $P = 1.2 \times 10^{-1}$ mbar (Experiment **6**) and a dynamic vacuum of $P = 1.2 \times 10^{-1}$ mbar (Experiment **5**), while only fine powders were obtained for the reaction under a dynamic vacuum of $P < 10^{-6}$ mbar (Experiments **3** and **13-18**).

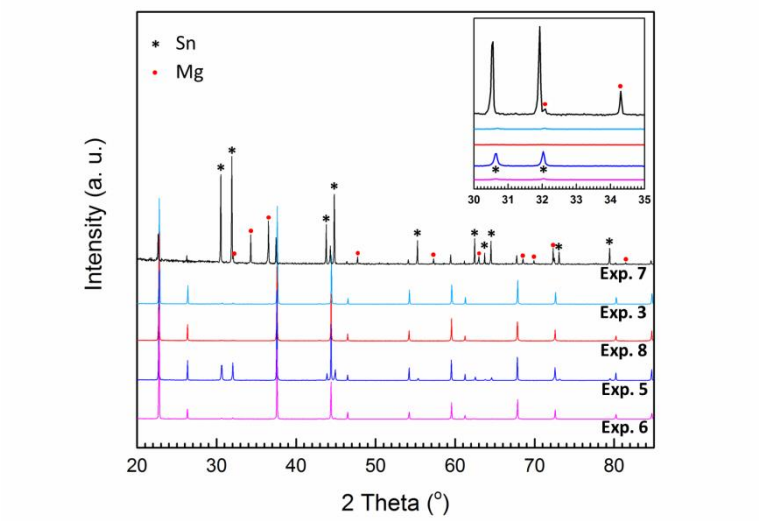

Figure 4. PXD patterns comparing the products obtained by varying pressures and vacuum conditions in experiments **3 (**P < 10^{-6} mbar; dynamic), **5** (P = 1.2 × 10^{-1} mbar; dynamic), **6** (P = 1.2 × 10^{-1} mbar; static), **7** (Ar at 1.002 bar) and **8** (P < 10^{-6} mbar; static), respectively; (Inset: PXD patterns from 30 – 37° 2θ, highlighting principal Sn (black marker) and Mg (red marker) impurity peaks).

Effect of MW Irradiation Time

Reactions under a Static Vacuum of P < 10^{-6} mbar

Experiments employing different MW irradiation times under a static vacuum of P < 10^{-6} mbar, ranging from 5 s to 1 min (Experiments **8-12**, Table **1**), were performed to study the evolution of the morphology, the progress of the reaction and the role of plasma in the ultrafast MW synthesis of Mg_2Sn. Plasmas were initiated within seconds in all the reactions. An irradiation time of just 5 s (**9**) is adequate for the formation of a significant amount of Mg_2Sn (63.8(7) wt%, with unreacted Mg 23.2(7) wt% and Sn 12.9(7) wt% constituting the balance of the sample) (Table **1**, Figures **5a, 5b** and **S7**). An Mg_2Sn phase fraction of 81.3(8) wt% could be achieved by increasing the irradiation time to 10 s (**10**). Thereafter, increasing the MW irradiation time to 30 s (**11**) and 45 s (**12**) increases the purity of Mg_2Sn to 99.22(7) wt % and 99.46(7) wt %, respectively; all the products were exclusively fine powders (*i.e.* containing no larger pieces as observed in experiment **8**). According to the Rietveld refinement data (Table **1**), the lattice parameters for each of the Mg_2Sn samples (**8-12**) are comparable irrespective of synthesis time, indicating that the MW irradiation times investigated have no significant effect on the crystal structure of Mg_2Sn.

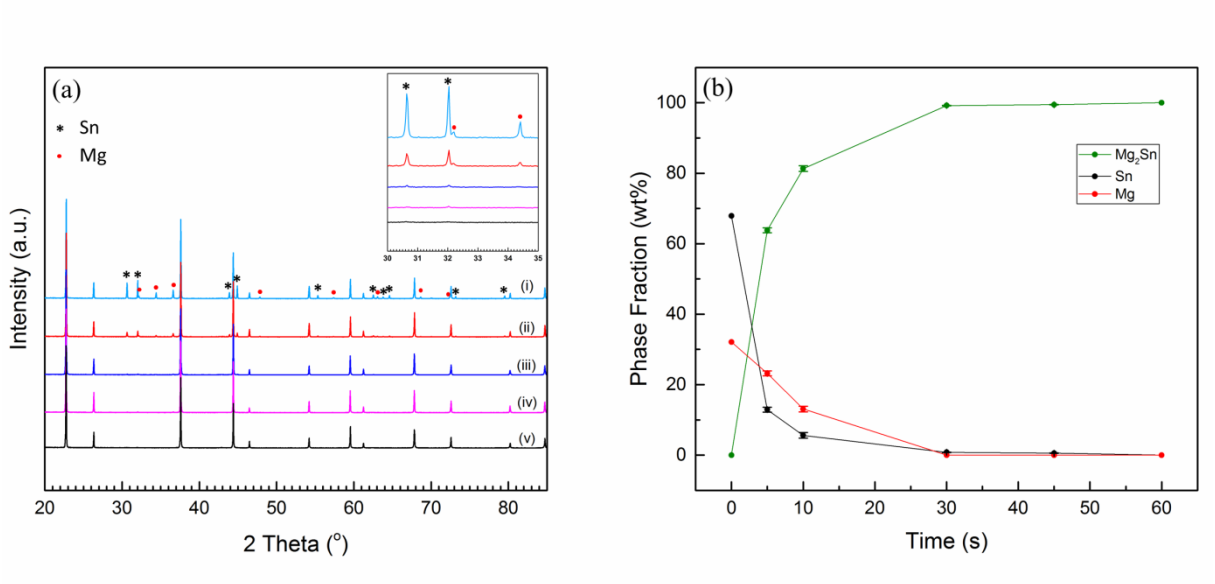

Figure 5. (a) PXD patterns of products from experiments **8**-**12**, obtained under a static vacuum (P <10^{-6} mbar) with MW irradiation times of (i) 5s, (ii)10 s, (iii) 30 s, (iv) 45s and (v) 60 s (Inset: PXD patterns from 30 – 35° (2θ) highlighting principal Sn (black marker) and Mg (red marker) impurity peaks); (b) Plot of phase fractions (wt%) as a function of MW irradiation times.

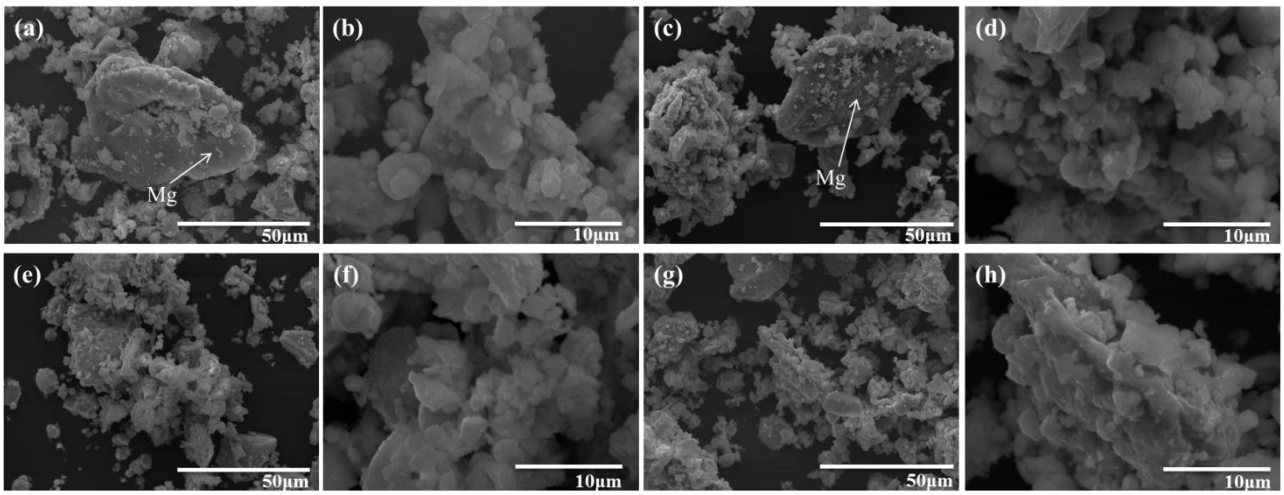

Figure 6.SEM images of the products from experiments **8**-**12**, obtained under a static vacuum of P <10^{-6} mbar with a MW irradiation time of (a, b) 5s; (c, d) 10 s; (e, f) 30 s; and (g, h) 45 s, respectively.

SEM images of the samples synthesised after 5 s and 10 s reveal the presence of fine micron-sized and submicron-sized spheres (which were possibly generated by the interactions caused by the plasma) and irregular micron-sized particles (Figures **6b**, **6d**, **S8b**, and **S9b**). Some large unreacted Mg particles could also be found according to EDX spectra (Figures **6a**, **6c**, **S8e-h**, and **S9e-h**), which is consistent with the presence of the Mg impurities in the PXD patterns (Figure **5a**). SEM images of samples synthesised using MW irradiation times of 30 s and 45 s reveal the products were composed of fine powders with particle sizes ranging from

the submicron regime to ~20 μm across (Figures **6e-h** and **S10**). The EDX spectra taken from each of these two samples (**11** and **12**) confirmed the Mg_2Sn stoichiometry (Figure **S10**).

Reactions under a Dynamic Vacuum of P < 10^{-6} mbar

The effect of altering the MW irradiation time from 5 to 80 s (Experiments **3**, **13-18**) was also investigated for syntheses performed under a dynamic vacuum (P < 10^{-6} mbar). Similar to the experiments performed under a static vacuum (P < 10^{-6} mbar), plasma was initiated within a few seconds. An irradiation of 5 s (**13**) led to the formation of Mg_2Sn (74.6(9) wt%) with the presence of more Mg (17.3(9) wt%) than Sn (8.1(9) wt%) (Figures **7a** and **7b**, Table **1**). The phase purity of Mg_2Sn could be improved to 80.4(8) wt% by increasing the irradiation time to 10 s (**14**). Figures **8a-d** show the morphology of samples obtained after 5 s and 10 s of irradiation. The samples were mainly composed of irregular particles of Mg_2Sn approximately 1-10 μm across and large unreacted Mg particles. There was also evidence of the existence of some spherical particles (from submicron size to micron size), which are similar to those in Figures **6b&d**. An irradiation time of 30 s (**15**) led to an Mg_2Sn phase fraction of 91.4(6) wt% and a decrease of Mg phase fraction to 5.8(6) wt%. None of the large unreacted Mg particles observed at shorter irradiation times could be found according to the SEM and EDX data. Mg impurities in the sample irradiated for 30 s were confirmed to be small particles approximately 10 μm across (Figures **8e** and **S15**).

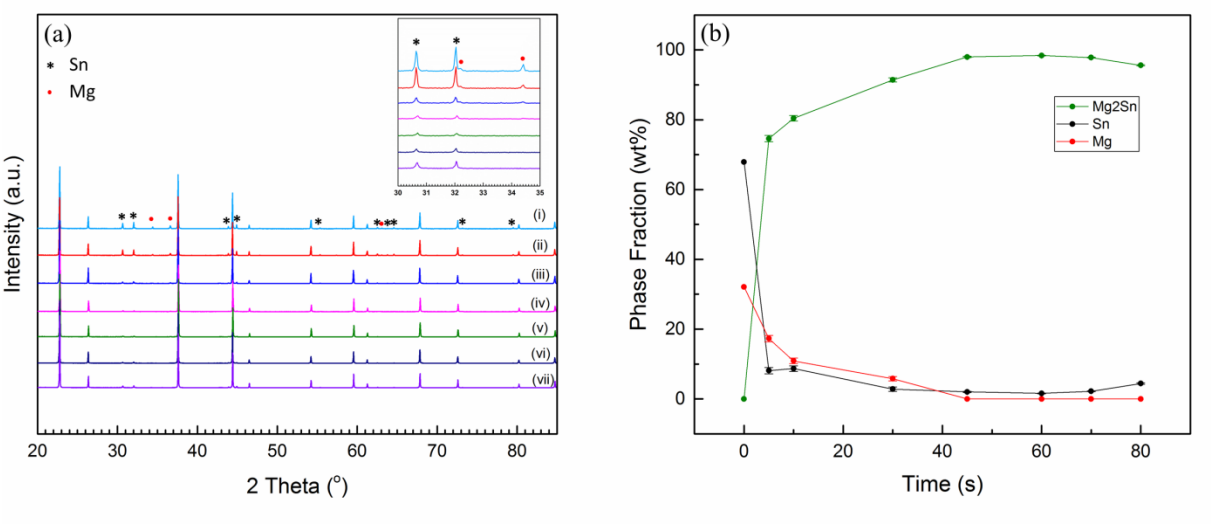

Figure 7.(a) PXD patterns of products from experiments **13-18** obtained under a dynamic vacuum (P <10^{-6} mbar) with MW irradiation times of (i) 5s, (ii)10 s, (iii) 30 s, (iv) 45s, (v) 60 s, (vi) 70 s and (vii) 80 s (Inset: PXD patterns from 30 – 35° (2θ) highlighting principal Sn (black markers) and Mg (red markers) impurity peaks); (b) Plot of phase fractions (wt %) of Mg_2Sn, Sn and Mg as a function of MW irradiation time.

Longer reaction times (t > 30 s) led to higher-purity Mg_2Sn without the presence of residual Mg (Table **1**). A highest Mg_2Sn purity of 98.4(1) wt% could be observed for the 60 s reaction, whereas the purity of Mg_2Sn slightly decreased to 97.8(1) wt% and 95.6 (2) wt% when the irradiation time was subsequently increased to 70 s (**17**) and 80 s (**18**), respectively (Figure **7b**). This apparent decrease in purity might be attributed to the loss of further Mg by sublimation/deposition such that residual Sn impurity in the solid product was proportionally greater (Figure **7b**). The probable decomposition of Mg_2Sn at temperatures above its melting point, may also lead to the transformation of Mg to the gas (or plasma) phase as seen in Supporting Information Video **2**. SEM images (Figures **8g, 8h** and **S16a**) show that samples irradiated for 45 – 80 s are mainly composed of micron-sized particles with minor amounts of irregular submicron-sized spheres or fragments. EDX spectra (Figure **S16b**) taken from both these types of particles confirm that the Mg:Sn molar ratios are in close agreement with the expected Mg_2Sn stoichiometry.

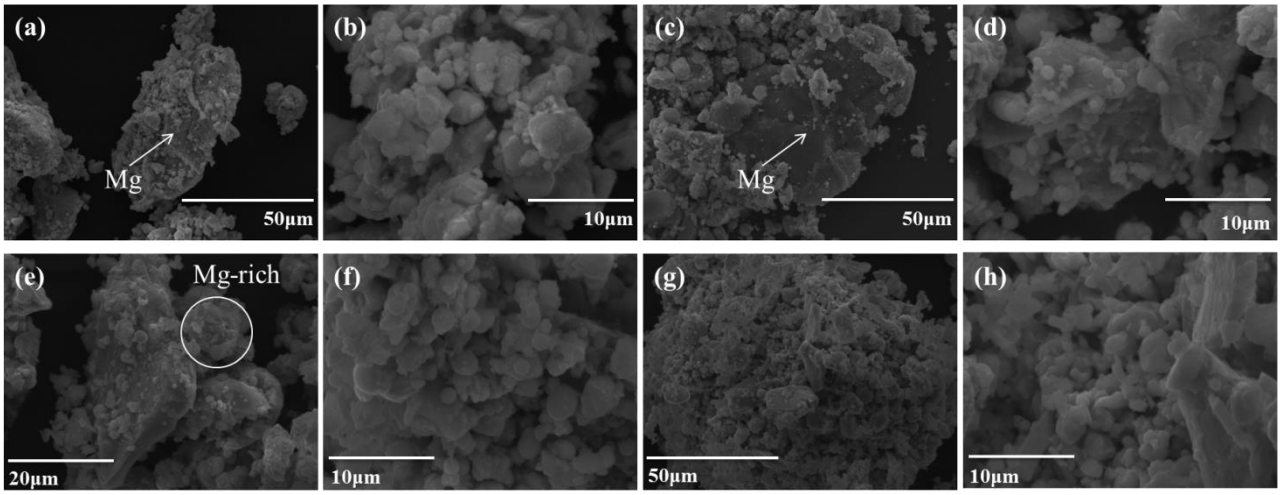

Figure 8.SEM images of the products from experiments **13**-**18**, obtained under a dynamic vacuum (P $<10^{-6}$ mbar) with MW irradiation times of (a, b) 5s; (c, d) 10 s;(e, f) 30 s; and (g, h) 45 s.

Discussions

MW irradiation of individual Mg and Sn powders under vacuum in this work (Section **3.1** and **3.2**) indicate that both elemental powders should couple well with MWs and generate plasma (Figure **S4**, Figure **S5**, Supporting Information Videos **3** and **4**) under appropriate conditions. The plasmas generated by the high-frequency electromagnetic field were observed to play an integral role in the ultrafast synthesis of Mg_2Sn. In this respect, the

synthetic conditions are rather different from those reported previously for microwave-induced plasma (MIP) syntheses [56], which exploit a low-pressure gas (*e.g.* Ar, H_2, NH_3, O_2, Cl_2 and H_2S) to generate an inert or reactive plasma that can thermally drive solid-state reactions [57]. (In fact, the quenching of the plasma due to pressure fluctuations in MIP reactions can be challenging and separating by-products from the final product is not trivial.) The plasma in our synthesis of Mg_2Sn is most likely generated *by the solid metal reactants themselves* (Figures **S4** and **S5**, Supporting Information Videos **3**-**5**), with the extent of the plasma controlled by adjusting the nature and magnitude of the external gas pressure; one might differentiate from MIP in terms of a "Microwave Induced Metal Plasma (MIMP)" synthesis.

Mg and Sn plasmas

Sn plasma has been widely generated by high-intensity laser pulses in a vacuum environment (with the first pulse evaporating Sn droplets while the second generates Sn plasma) to produce extreme-ultraviolet (EUV) light sources [58, 59]. Notably, up to 13 electrons in the intense heat of the Sn plasma could be lost per Sn atom with specific colours attributable to each of the possible charged states, resulting in a complex light emission [60]. The heating behaviour of Sn irradiated by MWs in an ambient atmosphere was studied by Buchelnikov *et al.* After an initial period of rapid heating, the Sn sample reached a temperature plateau followed by a further rapid heating phase after initiation of a spark-discharge [61]. However, to the best of our knowledge, Sn plasma generated by MWs under reduced pressure (vacuum) has not been reported before. It should be noted that, due to the low MP of Sn (231.93 $^{\circ}$C), the heating of Sn in the liquid state by MWs is likely to be unavoidable. Even though the heating mechanism of liquid Sn by MWs is not well-established, both our experiments (Figure **S5**) and the study of Buchelnikov *et al.* indicate that MWs can heat Sn rapidly above its melting point [61]. Compared with Sn, Mg presents a higher MP (650 $^{\circ}$C) but, conversely a much higher vapour pressure than Sn at the same temperature [59] (Figure **S3**); hence Mg requires a much less effective vacuum to evaporate than Sn. Mg vapours have been reported to generate a green plasma under vacuum conditions by MW irradiation from 580 $^{\circ}$C and above [62, 63]. It should also be noted that the direct evaporation (sublimation) of solid Mg to gaseous Mg (Figure **S4**) has also been reported in conventional high temperature syntheses of Mg_2Sn [20, 21, 22].

Although different charged states of the metal cations exhibit different colours, in this study, Sn consistently produced bright purple plasma when irradiated independently (Supporting Information Video **4**), while Mg generated purple plasma within the first *ca.* 15 s which became green on further heating (Supporting Information Video **3**). The latter green plasma is similar to previous observations of Mg in a MW field under vacuum [62, 63]. In this case, the fluctuation in colour with time of the Mg plasma may come from the change of the corresponding charged states of Mg cations. However, another reason for the observed variations may be attributed to the microplasma caused by the ionisation of the surrounding medium (residual Ar in this case) by electric discharge from the metal surface in a MW field. Typically, a purple emission from Ar plasma in the near UV region (400-480 nm) is produced under these circumstances [64, 65]. To evaluate the influence of plasma from residual Ar gas, a control experiment was performed in which SiC (acting as a thermally stable MW susceptor) was irradiated under a static vacuum ($P < 10^{-6}$ mbar) (Supporting Information Video **5**). Unlike when Mg or Sn reactants were irradiated (Supporting Information Videos **1**-**4**), any plasma that formed was purple and dissipated gradually. This strongly indicates that the plasmas generated in the Mg-Sn reactions are formed primarily by the metal reactants themselves rather than from residual Ar gas, which in turn promote the ultrafast synthesis process.

Hypothetical Mechanism for the MW Synthesis of Mg_2Sn

A simplified representation of the proposed synthesis mechanisms of Mg_2Sn by MW irradiation is shown in the schematic in Figure **9**. The formation of Mg_2Sn in a MW field is likely to share some features with the nucleation-growth mechanism observed in the conventional thermal solid-state synthesis of Mg_2Sn [66], but contrasts significantly in other respects. As fine metal particles, Mg and Sn powders couple efficiently with MWs and heat rapidly as a result. This is to be expected from ohmic heating, given that the MW penetration depth is of the same order as the particle diameter [32, 33] and that such behaviour was observed for each metal independently as described above. We assume that the melting of Sn and the ionisation of residual Ar occurs within seconds and that vapours of Mg and Sn are subsequently generated rapidly under vacuum conditions. The vapours will form plasmas (due to the relatively low ionisation energies of the outer shell electrons of the metals [62, 63]) containing Mg and Sn cations. Once plasmas form, the mode of heating should change markedly. The motion of the charged species is influenced by both the high-frequency *electrical* and *magnetic* field of the MWs. This leads to rapidly increased cation diffusion

rates and an even faster transport of electrons, giving rise to rapid heating, mass transport and enhanced reaction kinetics. Thus, the MW reaction process can involve: (a) the interaction between Mg and Sn plasmas; (b) the diffusion of the Mg plasma components into the liquid phase of Sn; (c) the interaction of the Sn plasma components with Mg particles/droplets (for example, solid Mg with a possible liquid "shell" coating); (d) dissolution of Mg in liquid Sn, where this dissolution is likely to be facilitated by the increasing solubility with temperature. In this final case, given the rapid rise in reaction temperature, the rate of this dissolution is likely to be greater than in conventional thermal reactions, which would promote the nucleation of Mg_2Sn at the Mg – Sn interface. Due to the heightened dynamics of plasmas governed by the high-frequency (2.45 GHz) MW field, it might be anticipated that the plasma-directed routes (a) – (c) would dominate the rapid kinetics of the Mg_2Sn MW synthesis from the solid elements over such short timescales.

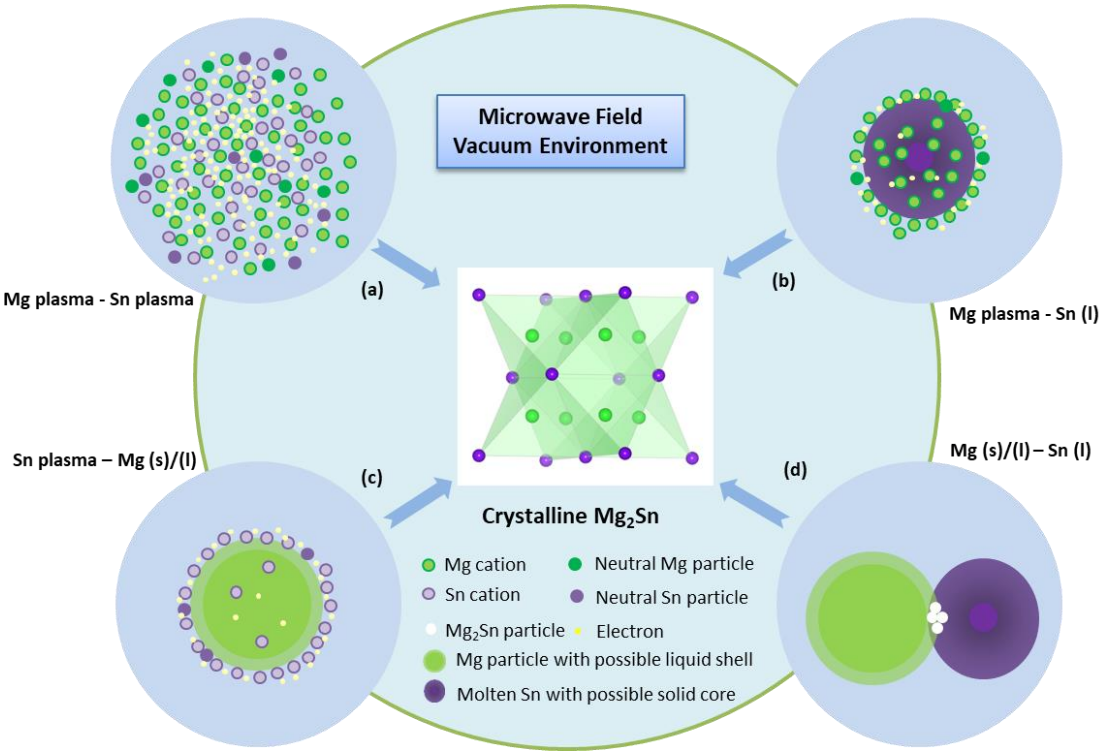

Figure 9. Hypothetical reaction routes in the MW synthesis of Mg_2Sn.

The metastable "high pressure" modification of Mg_2Sn previously reported in the literature [23 - 27] was not observed in any of the MW-synthesised products. In this study, the refined structures of each of the Mg_2Sn samples synthesised under different conditions match unequivocally with the cubic antifluorite structure [50]. This is perhaps unsurprising considering that the hexagonal form reverts to the cubic antifluorite at 600 ˚C and ambient pressure in any case [27]. Which of the above reaction routes, if any, is preferred requires

further investigation and would benefit from *in situ* experiments. Indeed, the interaction of Mg_2Sn itself with the MW field could be explored further given the alloy's nature as a narrow band gap semiconductor.

Effect of Experimental Parameters on the MW Synthesis of Mg_2Sn

Although both metallic, the variations in the chemical and physical properties of Mg and Sn, as well as their different particle sizes, can explain why the two elements might couple quite differently with MWs. These differences lead to inevitable variation in heating rates, vaporisation rates and plasma generation rates. This, in turn, means that the purity and morphology of the final products would be intimately affected by the synthesis parameters.

An excess of 15 mol% Mg is needed to obtain an Mg_2Sn product of high purity. Even with this excess of Mg, almost negligible amounts of Mg_2Sn was formed under Ar at atmospheric pressure, with no evidence of the melting-solidification of Sn observed (Experiment **19** and **7**). Even at elevated temperature, (initially) ambient pressure would not be sufficient for the vaporisation of either Mg or Sn and the consequent formation of plasmas was hindered. Conversely, the result from Experiment **7** implies the significance of plasma formation for the MW reaction of the solid state reactants to occur. As discussed in Sections **3.2** and **4.2**, the plasma would not only provide an additional heat source (inducing a fast heating rate) but also facilitate rapid reaction kinetics because of the enormously enhanced diffusion rates of ions in the gaseous state over the solid or liquid states. By comparison, in experiments performed under either dynamic or static vacuum conditions ($P < 10^{-6}$ mbar) - with the formation of plasma (Experiment **9** & **13**) - consistently high yields of Mg_2Sn could be obtained in just 5 s of MW irradiation, emphasising the ultrafast kinetics in the *MIMP* reaction. The submicron sized particles generated in the final products attest to the fact that plasma will generate fine particles even without intimate physical contact between precursors [35].

The pressure conditions have important effects on the vaporisation behaviour of Mg and Sn. In static vacuum experiments ($P < 10^{-6}$ mbar), the pressure in the tube would naturally increase due to the thermal expansion of residual Ar and the accumulation of Sn and Mg vapours during the reaction. This pressure increase would in turn mediate the vaporisation rates of Mg and Sn, influencing plasma formation and the purity of the final products. Under dynamic vacuum conditions ($P < 10^{-6}$ mbar), there is no such increase in pressure and the vaporisation of Mg and Sn is not hindered (Figures **S4** and **S5**). A large proportion of Mg

will enter the vapour phase with an increased likelihood of forming plasma. This vaporised Mg could thus re-condense/redeposit on the cooler walls of the quartz tube outside the reaction zone or even react with the quartz tube in the hotter irradiated region. This may be one reason why synthesis under a static vacuum (*e.g.* $P < 10^{-6}$ mbar, 60 s, Experiment **8**) produced products of higher purity than from dynamic vacuum experiments (*e.g.* $P < 10^{-6}$ mbar, 60 s, Experiment **3**). However, since plasma formation was observed to be both more rapid and more sustained under dynamic vacuum conditions (Supporting Information Videos **2** and **3**), in principle the products are more likely to be composed of fine powders rather than large metallic particles.

At the other extreme, some conditions are far more likely to yield impure products. For example, under a dynamic vacuum of $P = 1.2 \times 10^{-1}$ mbar, the vaporisation of Mg is likely to be much faster than that of Sn due to the higher volatility of the former (Figures **S4** and **S5**), leading to a high content of Sn impurity in the solid product. Hence, modifying the vacuum conditions significantly influences the vaporisation equilibrium of Mg and Sn, which is a major determinant in plasma formation and the purity of the stannide product.

For syntheses performed under a static vacuum ($P < 10^{-6}$ mbar), an irradiation time of 30 - 60 s is necessary to complete the reaction. However, a relatively long irradiation time of 60 s led to the presence of larger particles in the final products (Figure **2c**). This can be attributed to the melting and sintering of the material under longer MW irradiation times. By comparison, for equivalent reactions under a dynamic vacuum ($P < 10^{-6}$ mbar), an irradiation time of 45 - 60 s led to high-purity Mg_2Sn, but increasing the MW irradiation time further tended to affect the purity of the final products adversely. High temperature over long irradiation times might not only result in loss of gaseous reactants but might also lead to the melting of Mg_2Sn itself with its subsequent vaporisation and de-alloying of Mg from the compound [20].

To the best of our knowledge, definitive characterisation techniques to investigate the interaction of plasmas during solid-state MW synthesis have not been previously reported in the literature. The study of the physical conditions inside the reactor during synthesis are also critical, and advanced methods are required if one is to measure the temperature and potential distribution of matter without perturbing the MW field. Challenges exist not only in finding suitable time-resolved non-destructive methods to study the interactions between plasmas and the electromagnetic field but also in implementing those needed to study the formation

mechanism of the solid product. Among the possible options, *in-situ* spectroscopy (optical, acoustic emission), synchrotron XRD or *in-situ* Neutron diffraction could be potentially integrated with a MW reactor setup for further investigations [2-5, 58, 60]. The reflected power of MW from the solid reactants/products and especially the formed plasma phase(s) back to the MW source needs to be measured in future studies, as the plasma phase(s) might exhibit influence on the amount of reflected MW and the effective power for the proceeding of reaction. Moreover, the basic physics of the interaction between MWs and the reactant, intermediate and product materials needs to be better understood and related high-accuracy simulations are likely to be essential. Further, the experimental configuration used in the present study provided no means to measure the absorbed or reflected power and a bespoke single mode cavity reactor for *in situ* measurements would incorporate such a capability to enable measurement of power with time and temperature. We intend to address some of these fundamentally important issues in our further studies, establishing the boundaries for *MIMP* synthesis. We will also measure the properties of Mg_2Sn and similar materials synthesised by these routes and determine how synthesis variables impact on performance.

Conclusions

A simple, ultrafast and energy-efficient MW synthesis route to Mg_2Sn was established, developed and optimized. Phase-pure stannide (which is often elusive both by conventional heating and by other methods) can be produced as a result. Fine powders of both Mg and Sn couple well with MWs under vacuum and high yields of Mg_2Sn could be obtained in 5 seconds of irradiation under a vacuum of $P < 10^{-6}$ mbar. The formation of plasmas is fundamental in the MW synthesis providing heat, dictating reaction kinetics and determining the microstructure of the alloy. Unlike other microwave-induced plasma syntheses, the metals themselves provide a source of reactive plasma. This Microwave Induced Metal Plasma (*MIMP*) method should be readily adaptable to other members of the Mg_2X (X = Si, Ge) intermetallic antifluorite family and indeed to other alloys more broadly.

Supporting Information

Additional experimental details; Raman and TG-DTA data analyses; Experimental data from the MW irradiation of individual reactants; Rietveld refinement data for Mg_2Sn samples; SEM/EDS data for Mg_2Sn samples; Additional experimental data for an Mg:Sn 2.4:1 static vacuum sample; Videos of selected MW reactions in real time (.mov format).

Acknowledgements

The authors thank the China Scholarship Council and University of Glasgow for the co-funding of a studentship for ZF and the University of Glasgow for a Lord Kelvin-Adam Smith (LKAS) Scholarship for MDC. Mr. Hallam Davis, Mr. Nicolás Flores Gonzalez and Mr. James Gallagher are thanked for their assistance with the vacuum system, TG-DTA and SEM – EDX, respectively.

References

[1] Chu, S.; Cui, Y.; Liu, N. The Path Towards Sustainable Energy. *Nat. Mater.* **2017,** 16(1), 16.
[2] Kitchen, H. J.; Vallance, S. R.; Kennedy, J. L.; Tapia-Ruiz, N.; Carassiti, L.; Harrison, A.; Whittaker, A. G.; Drysdale, T. D.; Kingman, S. W.; Gregory, D. H. Modern Microwave Methods in Solid-State Inorganic Materials Chemistry: from Fundamentals to Manufacturing. *Chem. Rev.* **2014,** 114(2), 1170-1206.
[3] Vallance, S. R.; Kingman, S.; Gregory, D. H. Ultra-rapid Materials Processing: Synthesis of Tungsten Carbide, WC, in Sub-minute Timescales. *Adv. Mater.*, **2007**, 19, 138-142.
[4] Vallance, S. R.; Kingman, S.; Gregory, D. H. Ultra-rapid Processing of Refractory Carbides; 20 s Synthesis of Molybdenum Carbide, Mo_2C. *Chem. Commun.*, **2007**, 742-744.
[5] Carassiti, L.; Jones, A.; Harrison, P.; Dobson, P. S.; Kingman, S.; MacLaren, I.; Gregory, D. H. Ultra-rapid, Sustainable and Selective Synthesis of Silicon Carbide Powders and Nanomaterials via Microwave Heating.", *Energy Env. Sci.*, **2011**, 4, 1503 – 1510.
[6] Zhou, D.; Liu, J.; Xu, S.; Peng, P. Thermal Stability and Elastic Properties of Mg_2X (X= Si, Ge, Sn, Pb) Phases from First-Principle Calculations. *Comp. Mater. Sci.* **2012,** 51(1), 409-414.
[7] Zhang, L. Synthesis and Thermoelectric Properties of Mg_2Si-Mg_2Sn Solid Solutions for Waste Heat Recovery. PhD. Dissertation, The University of Texas at Austin, 2015.
[8] Liu, W.; Tan, X.; Yin, K.; Liu, H.; Tang, X.; Shi, J.; Zhang, Q.; Uher, C. Convergence of conduction Bands as a Means of Enhancing Thermoelectric Performance of n-type $Mg_2Si_{1-x}Sn_x$ Solid Solutions. *Phys. Rev. Lett.* **2012,** 108(16), 166601.
[9] Zaitsev, V. K.; Fedorov, M. I.; Gurieva, E. A.; Eremin, I. S.; Konstantinov, P. P.; Samunin, A. Y.; Vedernikov, M.V. Highly Effective $Mg_2Si_{1-x}Sn_x$ Thermoelectrics. *Phys. Rev. B*. **2006,** 74, 045207.
[10] Fedorov, M. I.; Zaitsev, V. K.; Isachenko, G. N. High Effective Thermoelectrics Based on the Mg_2Si-Mg_2Sn Solid Solution. *Solid State Phenom.* **2011,** 170, 286-292.
[11] Zhang, Q.; He, J.; Zhu, T. J.; Zhang, S. N.; Zhao, X. B.; Tritt, T. M. High Figures of Merit and Natural Nanostructures in $Mg_2Si_{0.4}Sn_{0.6}$ Based Thermoelectric Materials. *Appl. Phys. Lett.* **2008,** 93(10), 102109.
[12] Yi, S.; Attari, V.; Jeong, M.; Jian, J.; Xue, S.; Wang, H.; Arroyave, R.; Yu, C. Strain-Induced Suppression of the Miscibility Gap in Nanostructured Mg_2Si–Mg_2Sn Solid Solutions. *J. Mater. Chem. A*. **2018,** 6, 17559-17570.
[13] Sankhla, A.; Patil, A.; Kamila, H.; Yasseri, M.; Farahi, N.; Mueller, E.; Boor, J. D. Mechanical Alloying of Optimized Mg_2(Si, Sn) Solid Solutions: Understanding Phase Evolution and Tuning Synthesis Parameters for Thermoelectric Applications. *ACS Appl. Energy Mater.* **2018,** 1(2), 531-542.
[14] Jin, Y.; Feng, Z.; Ye, L.; Yan, Y.; Wang, Y. Mg_2Sn: a Potential Mid-Temperature Thermoelectric Material. *RSC Adv.* **2016,** 6, 48728-48736.
[15] Udono, H.; Tajima, H.; Uchikoshi, M.; Itakura, M. Crystal Growth and Characterization of Mg_2Si for IR-Detectors and Thermoelectric Applications. *Jpn. J. Appl. Phys.* **2015,** 54.07, 07JB06.
[16] Nguyen, D. T.; Song, S. W. Magnesium Stannide as a High-Capacity Anode for Magnesium-Ion Batteries. *J. Power Sources.* **2017,** 368, 11-17.
[17] Huang, B.; Pan, Z.; Su, X.; An, L. Tin-Based Materials as Versatile Anodes for Alkali (Earth)-Ion Batteries. *J. Power Sources.* **2018,** 395, 41-59.
[18] Mortazavi, M.; Soon, E.; Medhekar, N. V. First Principles Insights into Amorphous Mg_2Sn Alloy Anode for Mg-ion Batteries. *ChemRxiv*, [Online] **2018,** http://doi.org/10.26434/chemrxiv.6462887.v1 (accessed Aug 05, 2019).

[19] Niu, J.; Gao, H.; Ma, W.; Luo, F.; Yin, K.; Peng, Z.; Zhang, Z. Dual Phase Enhanced Superior Electrochemical Performance of Nanoporous Bismuth-Tin Alloy Anodes for Magnesium-Ion Batteries. *Energy Storage Mater*. **2018,** 14, 351-360.
[20] Yaghoobnejad Asl, H.; Fu, J.; Kumar, H.; Welborn, S. S.; Shenoy, V. B.; Detsi, E. In Situ Dealloying of Bulk Mg_2Sn in Mg-Ion Half Cell as an Effective Route to Nanostructured Sn for High Performance Mg-Ion Battery Anodes. *Chem. Mater.* **2018,** 30(5), 1815-1824.
[21] Hu, F. Synthesis and Characterization of Magnesium-Silicon and Magnesium-Tin Solid Solutions for Thermoelectric Applications. MSc. Dissertation, Texas A&M University, 2012.
[22] Zhang, Q.; Lu, Q.; Yan, Y.; Su, X.; Tang, X. Ultrafast Synthesis and Related Phase Evolution of Mg_2Si and Mg_2Sn Compounds. *Journal of Elec. Mater.* **2017,** 46, 3172-3181.
[23] Clark, C. R.; Wright, C.; Suryanarayana, C.; Baburaj, E. G.; Froes, F. H. Synthesis of Mg_2X (X= Si, Ge, or Sn) Intermetallics by Mechanical Alloying. *Mater. Lett.* **1997,** 33(1-2), 71-75.
[24] Kim, H.; Kim, Y. J.; Kim, D. G.; Sohn, H. J.; Kang, T. Mechanochemical Synthesis and Electrochemical Characteristics of Mg_2Sn as an Anode Material for Li-Ion Batteries. *Solid State Ionic.*, **2001,** 144(1-2), 41-49.
[25] Aizawa, T.; Song, R. Mechanically Induced Reaction for Solid-State Synthesis of Mg_2Si and Mg_2Sn. *Intermetallics.* **2006,** 14(4), 382-391.
[26] Larcher, D.; Prakash, A. S.; Saint, J.; Morcrette, M.; Tarascon, J. M. Electrochemical Reactivity of Mg_2Sn Phases with Metallic Lithium. *Chem. Mater.* **2004,** 16(25), 5502-5511.
[27] Urretavizcaya, G.; Meyer, G. O. Metastable Hexagonal Mg_2Sn Obtained by Mechanical Alloying. *J. Alloy Compd.* **2002,** 339(1-2), 211-215.
[28] Soni, P. R. Mechanical Alloying: Fundamentals and Applications; Cambridge Int Science Publishing: Cambridge, 2000.
[29] An, T. H.; Choi, S. M.; Kim, I. H.; Kim, S. U.; Seo, W. S.; Kim, J. Y.; Park, C. Thermoelectric Properties of a Doped Mg_2Sn System. *Renew. Energ.* **2012,** 42, 23-27.
[30] Horikoshi, S.; Schiffmann, R. F.; Fukushima, J.; Serpone, N. Microwave Chemical and Materials Processing; Springer: Singapore, 2018.
[31] Gupta, M. and Leong, E. W. W. Microwaves and Metals; John Wiley & Sons: Singapore, 2008.
[32] Newnham, R. E.; Jang, S. J.; Xu, M.; Jones, F. Fundamental Interaction Mechanisms between Microwaves and Matter. *Ceramic Transactions.* **1991,** 21, 51-67.
[33] Whittaker, A. G.; Mingos, D. M. P. Microwave-Assisted Solid-State Reactions Involving Metal Powders. *J. Chem. Soc., Dalton Trans.***1995,** 12, 2073-2079.
[34] Mastrovito, C.; Lekse, J. W.; Aitken, J. A. Rapid Solid-State Synthesis of Binary Group 15 Chalcogenides Using Microwave Irradiation. *J. Solid State Chem.* **2007,** 180(11), 3262-3270.
[35] Lekse, J. W.; Stagger, T. J.; Aitken, J. A. Microwave Metallurgy: Synthesis of Intermetallic Compounds via Microwave Irradiation. *Chem. Mater*. **2007,** 19(15), 3601-3603.
[36] Kadhim, A.; Arshad, H.; Hassan, H. A. Effect of Se Substitution on Structural and Electrical Transport Properties of $Bi_{0.4}Sb_{1.6}Se_{3x}Te_{3(1-x)}$ Hexagonal Rods. *J. Electron. Mater.* **2013,** 42(6), 1017-1023.
[37] Agrawal, D. Microwave Sintering of Ceramics, Composites and Metallic Materials, and Melting of Glasses. *T. Indian Ceram. Soc.* **2006,** 65(3), 129-144.
[38] Mishra, R. R.; Rajesha, S.; Sharma, A. K. Microwave Sintering of Pure Metal Powders – a Review. *Int J Adv Mech Eng.* **2014,** 4(3), 315-322.
[39] Palchik, O.; Gedanken, A.; Palchik, V.; Slifkin, M. A.; Weiss, A. M. Microwave-Assisted Preparation, Morphological, and Photoacoustic Studies of the Na_4SnSe_4, $K_4Sn_2Se_6$, and $K_4Sn_3Se_8$, Zintl Molecular Sn–Se Oligomers. *J. Solid State Chem.* **2002,** 165(1), 125-130.
[40] Zhou, G.; Palchik, O.; Nowik, I.; Herber, R.; Koltypin, Y.; Gedanken, A. Microwave-Assisted Selective Preparation and Characterization of $Li_{21}Si_5$ and $Li_{17}Sn_4$. *J. Solid State Chem.* **2004,** 177(9), 3014-3020.
[41] Lei, Y.; Li, Y.; Xu, L.; Yang, J.; Wan, R.; Long, H. Microwave Synthesis and Sintering of TiNiSn Thermoelectric Bulk. *J. Alloy Compd.* **2016,** 660, 166-170.
[42] Lei, Y.; Cheng, C.; Li, Y.; Wan, R.; Wang, M. Microwave Synthesis and Enhancement of Thermoelectric Figure of Merit in Half-Heusler $TiNiSb_xSn_{1-x}$. *Ceram. Int.* **2017,** 43(12), 9343-9347.
[43] Lei, Y.; Wang, M.; Li, Y.; Gao, W.; Wan, R.; Cheng, C. Microwave Synthesis, Microstructure, and Thermoelectric Properties of Zr Substituted $Zr_xTi_{1-x}NiSn$ Half-Heusler Bulks. *Mater. Lett.* **2017,** 201, 189-193.
[44] Xia, Q.; Yi, J.; Peng, Y.; Luo, S.; Li, L. Microwave Direct Synthesis of MgB_2 Superconductor. *Mater. Lett.* **2008,** 62(24), 4006-4008.
[45] Zhou, S.; Bai, C. Microwave Direct Synthesis and Thermoelectric Properties of Mg_2Si by Solid-State Reaction. *T. Nonferr. Metal. SOC.* **2011,** 21(8), 1785-1789.
[46] Zhou, S.; Bai, C. Synthesis and Thermoelectric Properties of $Mg_2Si_{1-x}Sn_x$ Solid Solutions by Microwave Irradiation. *J. Cent. South. Univ.* **2012,** 19(9), 2421-2424.
[47] Savary, E.; Franck, G.; Marinel, S. Fast Synthesis of Nanocrystalline Mg_2Si by Microwave Heating: a New Route to Nano-Structured Thermoelectric Materials. *Dalton Trans.* **2010,** 39(45), 11074-11080.

[48] Robertson, W. D.; Uhlig, H. H. Chemical Properties of the Intermetallic Compounds Mg_2Sn and Mg_2Pb. *J. Electrochem. Soc.* **1949,** 96, 27-42.
[49] Barker, M.G.; Begley, M. J.; Edwards, P. P.; Gregory D. H.; Smith, S. E. Synthesis and Crystal Structures of the New Ternary Nitrides Sr_3CrN_3 and Ba_3CrN_3. *J. Chem. Soc., Dalton Trans.* **1996,** 1-5.
[50] Nikitin, E.N.; Tkalenko, E. N.; Zaitsev, V. K.; Zaslavskii, A. I.; Kuznetsov, A. K. A Study of the Phase Diagram for the Mg_2Si-Mg_2Sn System and the Properties of Certain of Its Solid Solutions. *Inorg. Mater*. **1968,** 4, 1656-1659.
[51] Swanson, H. E.; Eleanor, T.; Ruth, K. F. Standard X-ray Diffraction Powder Patterns. *National Bureau of Standards Circular (U. S.).* **1953,** 539, 1-95.
[52] Toby, B. H. EXPGUI, a Graphical User Interface for GSAS. *J. Appl. Cryst.* **2001,** 34(2), 210-213.
[53] Petricek, V.; Dusek, M.; Palatinus, L. Crystallographic Computing System JANA2006: General features. *Z. Kristallogr*. **2014,** 229(5), 345-352.
[54] Galkin, N. G.; Galkin, K. N.; Goroshko, D. L.; Chernev, I. M.; Shevlyagin, A. V.; Dozsa, L.; Osvath, Z.; Pecz, B. Non-Doped and Doped Mg Stannide Films on Si(111) Substrates: Formation, Optical, and Electrical Properties. *JPN J. Appl. Phys.* **2015,** 54(7S2), 07JC06.
[55] Chou, Y.; Morgan, A. J.; Hondow, N. S.; Brydson, R.; Douthwaite, R. E. Microwave-Induced Plasma Heating and Synthesis: In situ Temperature Measurement of Metal Oxides and Reactions to Form Ternary Oxides. *Dalton Trans.* **2010,** 39, 6062-6066.
[56] Suriwong, T.; Thongtem, S.; Thongtem, T. Solid-State Synthesis of Cubic ZnTe Nanocrystals Using a Microwave Plasma. *Mater. Lett.* **2009,** 63(24-25), 2103-2106.
[57] Brooks, D. J.; Douthwaite, R. E. Microwave-Induced Plasma Reactor Based on a Domestic Microwave Oven for Bulk Solid State Chemistry. *Rev. Sci. Instrum.* **2004,** 75(12), 5277-5279.
[58] Banine, V. Y.; Koshelev, K. N.; Swinkels, G. H. P. M. Physical Processes in EUV Sources for Microlithography. *J. Phys. D: Appl. Phys.* **2011,** 44(25), 253001.
[59] Yaws, C. L. Handbook of Vapor Pressure: Volume 4: Inorganic Compounds and Elements. Vol. 4; Gulf Professional Publishing: Houston, 1995.
[60] Torretti, F.; Windberger, A.; Ryabtsev, A.; Dobrodey, S.; Bekker, H.; Ubachs, W.; Hoekstra, R.; Kahl, E. V.; Berengut, J. C.; Lopez-Urrutia J. R. C.; Versolato, O. O. Optical Spectroscopy of Complex Open-4d-Shell Ions Sn^{7+} – Sn^{10+}. *Phys. Rev. A.* **2017,** 95, 042503.
[61] Buchelnikov, V. D.; Louzguine-Luzgin D. V.; Xie, G.; Li, S.; Yoshikawa, N.; Sato, M. Anzulevich, A. P.; Bychkov, I. V.; Inoue, A. Heating of Metallic Powders by Microwaves: Experiment and Theory. *J. Appl. Phys.* **2008,** 104(11), 113505.
[62] Wada, Y.; Fujii, S.; Suzuki, E.; Maitani, M.; Tsubaki, S.; Chonan, S.; Fukui, M.; Inazu, N. Smelting Magnesium Metal Using a Microwave Pidgeon Method. *Sci. Rep.* **2017,** 7, 46512.
[63] Kleiber, P. D.; Lyyra, A. M.; Heneghan, S. P.; Stwalley, W. C. Stimulated Emission in Laser-Pumped Magnesium Vapor. *J. Opt. Soc. Am. B.***1985,** 2,522-526.
[64] Menéndez, J. A.; Arenillas, A.; Fidalgo, B.; Fernandez, Y.; Zubizarreta, L.; Calvo, E. G.; Bermudez, J. M. Microwave Heating Processes Involving Carbon Materials. *Fuel Process. Technol.* **2010,** 91(1), 1-8.
[65] Norlén, G. Wavelengths and Energy Levels of Ar I and Ar II Based on New Interferometric Measurements in the Region 3 400-9 800 Å. *Phys. Scr.* **1973,** 8, 249.
[66] Nayeb-Hashemi, A. A.; Clark, J. B. The Mg − Sn (Magnesium-Tin) System. *Bulletin of Alloy Phase Diagrams*, **1984,** 5, 466-476.

Tables

Table 1. Experimental parameters and summary of morphology and structural parameters according to Rietveld refinement of the MW-synthesised products of Mg_2Sn

Experiment	Mg/Sn Molar Ratio [a]	Irradiation Time/s	Atmosphere	Morphology	Refined phase fractions / wt% Mg_2Sn, Sn, Mg	Mg_2Sn cell parameter, a / Å	Mg_2Sn density / g cm^{-3} [b]	*Goodness of fit*, χ^2
1	2.1:1	60	Dynamic vacuum P < 10^{-6} mbar	Fine powders	88.4(3), 11.6(3), 0	6.7651(1)	3.589	1.809
2	2.2:1	60	Dynamic vacuum P < 10^{-6} mbar	Fine powders	97.0(1), 3.0(1), 0	6.7648(3)	3.590	1.701
3	2.3:1	60	Dynamic vacuum P < 10^{-6} mbar	Fine powders	98.4(1), 1.6(1), 0	6.7657(3)	3.588	2.155
4	2.4:1	60	Dynamic vacuum P < 10^{-6} mbar	Fine powders	97.7(1), 2.3(1), 0	6.7650(2)	3.589	2.572
5	2.3:1	60	Dynamic vacuum P = 1.2×10^{-1} mbar	Metallic pieces & fine powders	78.6(4), 21.4(4), 0	6.7655(1)	3.589	1.919
6	2.3:1	60	Static vacuum P = 1.2×10^{-1} mbar	Metallic pieces & fine powders	97.3(3), 2.7(3), 0	6.7653(4)	3.589	2.590
7	2.3:1	60	Under Ar, P = 1 bar	Fine powders	12(1), 37(1), 51(1)	6.7636(2)	3.591	1.538
8	2.3:1	60	Static vacuum P < 10^{-6} mbar	Metallic pieces & fine powders	100, 0, 0	6.7653(1)	3.589	2.434
9	2.3:1	5	Static vacuum P < 10^{-6} mbar	Fine powders	63.8(7), 12.9(7), 23.2(7)	6.7643(3)	3.590	1.880
10	2.3:1	10	Static vacuum P < 10^{-6} mbar	Fine powders	81.3(8), 5.6(8), 13.1(8)	6.7640(1)	3.591	2.153
11	2.3:1	30	Static vacuum P < 10^{-6} mbar	Fine powders	99.22(7), 0.78(7), 0	6.7634(3)	3.592	1.973
12	2.3:1	45	Static vacuum P < 10^{-6} mbar	Fine powders	99.46(7), 0.54(7), 0	6.7635(3)	3.592	1.967
13	2.3:1	5	Dynamic vacuum P < 10^{-6} mbar	Fine powders	74.6(9), 8.1(9), 17.3(9)	6.7646(3)	3.590	1.679
14	2.3:1	10	Dynamic vacuum P < 10^{-6} mbar	Fine powders	80.4(8), 8.7(8), 10.9(8)	6.7636(3)	3.591	1.888
15	2.3:1	30	Dynamic vacuum P < 10^{-6} mbar	Fine powders	91.4(6), 2.8(6), 5.8(6)	6.7634(2)	3.592	1.767
16	2.3:1	45	Dynamic vacuum P < 10^{-6} mbar	Fine powders	98.0 (2), 2.0(2), 0	6.7660(2)	3.587	1.925
17	2.3:1	70	Dynamic vacuum P < 10^{-6} mbar	Fine powders	97.8(1), 2.2(1), 0	6.7638(2)	3.591	1.872
18	2.3:1	80	Dynamic vacuum P < 10^{-6} mbar	Fine powders	95.6(2), 4.4(2), 0	6.7646(2)	3.590	2.125
19	2.3:1	30	Under Ar, P = 1 bar	Fine powders	0, 46(1), 54(1)	-	-	1.657

a 148 mg of Sn powder was employed in all experiments. Masses of Mg powder of 64, 67, 70 and 73 mg corresponded to a Mg/Sn molar ratio of 2.1:1, 2.2:1, 2.3:1 and 2.4:1, respectively.

b as determined crystallographically.

Table 2. Crystallographic data obtained from the Rietveld refinement for Mg_2Sn powders from Experiment 8

Chemical Formula	**Mg_2Sn**
Crystal System	Cubic
Space Group	$Fm\bar{3}m$ (225)
Lattice Parameter, a /Å	6.7653(1)
Formula Weight /g mol^{-1}	669.200
Formula Units, Z	4
Calculated Density / g cm^{-3}	3.589
No. of Observations	6283
R_{wp}	0.1227
R_p	0.0841
χ^2	2.434

Table 3. Atomic parameters for Mg_2Sn powders from Experiment 8

Atom	**Wyckoff Symbol**	**x**	**y**	**z**	**$100*U_{iso}$ / Å^2**	**Occupancy**
Mg	8c	0.25	0.25	0.25	0.98(6)	0.998(6)
Sn	4a	0	0	0	0.36(2)	1

For Table of Contents Use Only

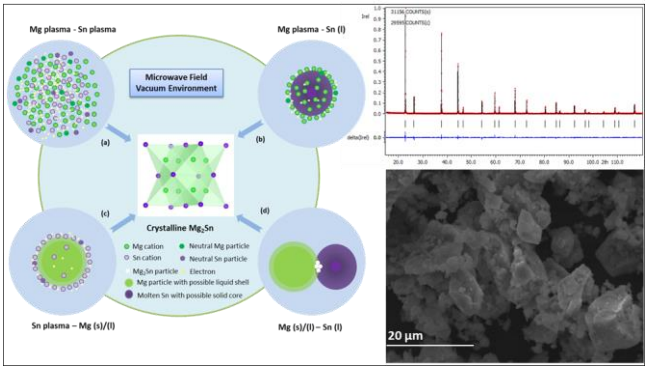

Microwave-induced metal plasma (*MIMP*) synthesis produces phase-pure Mg_2Sn in 1 minute at a fraction of the energy cost of conventional synthesis approaches.